

Carrier States and Ferromagnetism in Diluted Magnetic Semiconductors

Masao TAKAHASHI^{*} and Kenn KUBO¹

*Kanagawa Institute of Technology
1030 Shimo-Ogino, Atsugi-shi, 243-0292*

¹*Department of Physics, Aoyama Gakuin University
Sagamihara, Kanagawa 229-8558*

(Received May 4, 2019)

Applying the dynamical coherent potential approximation to a simple model, we have systematically studied the carrier states in $A_{1-x}\text{Mn}_x\text{B}$ -type diluted magnetic semiconductors (DMS's). The model calculation was performed for three typical cases of DMS's: The cases with strong and moderate exchange interactions in the absence of nonmagnetic potentials, and the case with strong attractive nonmagnetic potentials in addition to moderate exchange interaction. When the exchange interaction is sufficiently strong, magnetic impurity bands split from the host band. Carriers in the magnetic impurity band mainly stay at magnetic sites, and coupling between the carrier spin and the localized spin is very strong. The hopping of the carriers among the magnetic sites causes ferromagnetism through a *double-exchange (DE)-like* mechanism. We have investigated the condition for the DE-like mechanism to operate in DMS's. The result reveals that the nonmagnetic attractive potential at the magnetic site assists the formation of the magnetic impurity band and makes the DE-like mechanism operative by substantially enhancing the effect of the exchange interaction. Using conventional parameters we have studied the carrier states in $\text{Ga}_{1-x}\text{Mn}_x\text{As}$. The result shows that the ferromagnetism is caused through the DE-like mechanism by the carriers in the bandtail originating from the impurity states.

KEYWORDS: diluted magnetic semiconductors, exchange interaction, coherent potential approximation, carrier-induced ferromagnetism

§1. Introduction

For more than two decades diluted magnetic semiconductors (DMS's) have attracted much attention because of the combination of magnetic and semiconducting properties. In $A_{1-x}^{\text{II}}\text{Mn}_x\text{B}^{\text{VI}}$ -type (II-VI-based) DMS's, Mn impurities substituting for 2+ cations act as stable 2+ ions and therefore there are few carriers, making these DMS's insulators. It is widely accepted that in II-VI-based DMS's a carrier (s electron or p hole) moves over many sites while interacting with the localized (d) spins on Mn sites through the sp - d exchange interaction.¹⁾ The exchange interaction strongly enhances the effect of magnetic field on band splitting, leading to spectacular magneto-optical effects (e.g., giant Faraday rotation or Zeeman splitting). In recent years the attention has also been focused on III-V-based DMS's ($\text{Ga}_{1-x}\text{Mn}_x\text{As}$ and $\text{In}_{1-x}\text{Mn}_x\text{As}$) due to the high potential for new device applications. It is highly noteworthy that doping of Mn into GaAs and InAs leads to ferromagnetism, and interesting magneto-optical and magnetotransport phenomena. This ferromagnetism is generally called "carrier-induced ferromagnetism" because hole carriers introduced by Mn incorporation mediate the ferromagnetic coupling between Mn ions.²⁾ The microscopic mechanism for carrier-induced ferromagnetism is still controversial. The following properties, however, seem to be generally accepted as for (Ga,Mn)As: (i) Mn ions substitute randomly for Ga cations in the zincblende structure.²⁾ (ii) A Mn ion in GaAs gives rise to an acceptor level at about 0.113 eV above the valence band.³⁾ (iii) The Mn ion has highly localized d states with a magnetic moment of $\sim 5\mu_B$ (or $S = 5/2$).³⁻⁵⁾ (iv) The Mn-induced states near the Fermi energy play a key role

^{*} E-mail address: taka@gen.kanagawa-it.ac.jp

in the origin of ferromagnetism. According to photoemission studies,⁶⁻⁸⁾ X-ray absorption spectroscopy,⁹⁾ and band calculations,^{10,11)} those states are mainly created in As $4p$ orbits. (v) The p - d exchange interaction between the As $4p$ hole and the localized d spin is antiferromagnetic,^{12,13)} and its amplitude is not very different from that in II-VI-based DMS's.^{6,14)} (vi) Antisite defects (As ions sitting on Ga lattice site), for example, are common in semiconductor samples grown by low-temperature molecular beam epitaxy.¹⁵⁾ Many holes may be trapped not at Mn acceptors but at such defects, though we may expect one hole donated by a Mn atom. The density of the holes and that of the Mn ions are therefore regarded as separate sample-dependent quantities that are to be determined experimentally.

Since the fabrication of III-V DMS's much effort has been made on the elucidation of the origin of the ferromagnetism. To date, the Ruderman-Kittel-Kasuya-Yosida (RKKY) mechanism,¹⁶⁾ the double-exchange mechanism based on d electron hopping,¹⁷⁾ the spin-wave approximation for the kinetic-exchange model,¹⁸⁾ the double-resonance mechanism,¹⁹⁾ the Zener-model description,²⁰⁾ a theory based on the random-phase approximation and the coherent potential approximation,²¹⁾ and the coherent potential approach to a model with randomly distributed Ising spins²²⁾ have been proposed. To our knowledge, however, no systematic theoretical study on the carrier states in DMS's, in which both the exchange interactions and nonmagnetic attractive potentials exist, have been accomplished taking the effect of disorder into account.

In this study we aim to clarify the nature of carrier states in DMS's applying the dynamical coherent potential approximation (dynamical CPA) to a simple model. Furthermore, on the basis of the numerical calculation, we discuss the origin and the mechanism of the carrier-induced ferromagnetism in III-V DMS's.²³⁾

The main content and the organization of this paper are as follows. In §2, we briefly summarize the present model and the dynamical CPA. In §3 after a general consideration of the DMS's and the model parameters (§3.1), we first present the results for the carrier states in the DMS's with no nonmagnetic attractive potential: the case of the strong exchange interaction (§3.2) and the case of the moderate exchange interaction (§3.3). Then, based on the result we discuss the mechanism of carrier-induced ferromagnetism in DMS's (§3.4). The result of this study reveals that the double-exchange (DE)-like mechanism^{24,25)} is in effect to realize a high Curie temperature when the exchange interaction is strong enough to form a magnetic impurity band split from the host band. On the other hand, the RKKY mechanism may be relevant when the exchange interaction is so weak as not to produce a magnetic impurity band. The latter corresponds to the case of II-VI-based DMS's. As mentioned above, the strength of the p - d exchange interaction in III-V DMS's is not very different from that in II-VI DMS's. Then, what causes the ferromagnetism in III-V DMS ? The key lies in the attractive Coulomb potential between a p hole and a Mn acceptor center. In §3.5, we investigate the role of the attractive potential to elucidate the origin of the carrier-induced ferromagnetism in III-V DMS's. Section 4 is devoted to (Ga,Mn)As together with a comparison with (In,Mn)As. Concluding remarks are presented in §5.

§2. Basic consideration

2.1 Model Hamiltonian for a carrier in a DMS

In order to study the effect of the p - d exchange interaction between a carrier (p hole) and localized magnetic moments together with magnetic and chemical disorder in DMS's, we previously proposed a simple model.^{23,26)} In the model, the local potentials of nonmagnetic A ions in a semiconducting compound AB are substituted randomly, with mole fraction x , by the local potentials that include the exchange interactions between carrier spins and the localized spin moments on

magnetic M ions. Thus, the potential to which a carrier is subject at a site differs depending on whether the site is occupied by an A ion or an M ion. The Hamiltonian H is given by

$$H = \sum_{m,n,\mu} \varepsilon_{mn} a_{m\mu}^\dagger a_{n\mu} + \sum_n u_n, \quad (2.1)$$

where u_n is either u_n^A or u_n^M , depending on the ion species occupying the n site:

$$u_n^A = E_A \sum_{\mu} a_{n\mu}^\dagger a_{n\mu}, \quad (2.2)$$

$$u_n^M = E_M \sum_{\mu} a_{n\mu}^\dagger a_{n\mu} - I \sum_{\mu,\nu} a_{n\mu}^\dagger \boldsymbol{\sigma}_{\mu\nu} \cdot \mathbf{S}_n a_{n\nu}. \quad (2.3)$$

The notations here are conventional and the same as in the previous papers.^{23,26–28} Here, E_A (E_M) represents a nonmagnetic local potential at an A (M) site. We employ a local potential E_M although the real potential for a hole is an attractive screened Coulomb potential exerted by a Mn^{2+} acceptor center in III-V-based DMS's such as $\text{Ga}_{1-x}\text{Mn}_x\text{As}$. The exchange interaction between a carrier spin and the localized spin \mathbf{S}_n of the Mn site n is expressed by $-I a_{n\mu}^\dagger \boldsymbol{\sigma}_{\mu\nu} \cdot \mathbf{S}_n a_{n\nu}$, where $\boldsymbol{\sigma}_{\mu\nu}$ represents the element of the Pauli spin matrices.

2.2 Dynamical coherent potential approach

A carrier moving in a DMS described by Eq. (2.1) is subject to disordered potentials which arise not only from substitutional disorder but also from thermal fluctuations of d spins through the p - d exchange interaction. Furthermore, when magnetization arises, the effective potential for the carrier differs according to the orientation of the carrier's spin. In the dynamical coherent potential approximation (dynamical CPA),^{29,30} the disordered potential is taken into account in terms of the spin-dependent effective medium where a carrier is subject to a coherent potential Σ_\uparrow or Σ_\downarrow according to the orientation of its spin. The coherent potential Σ_\uparrow (Σ_\downarrow) is an energy (ω) dependent complex potential. Then, a carrier moving in this effective medium is described by the unperturbed Hamiltonian K :

$$K = \sum_{k\mu} (\varepsilon_k + \Sigma_\mu) a_{k\mu}^\dagger a_{k\mu}. \quad (2.4)$$

Thus, the perturbation term $V(=H-K)$ is written as a sum over each lattice site:

$$V = \sum_n v_n, \quad (2.5)$$

where v_n is either v_n^A or v_n^M , depending on the ion species occupying the n site:

$$v_n^A = \sum_{\mu} (E_A - \Sigma_\mu) a_{n\mu}^\dagger a_{n\mu}, \quad (2.6)$$

$$v_n^M = \sum_{\mu} (E_M - \Sigma_\mu) a_{n\mu}^\dagger a_{n\mu} - I \sum_{\mu,\nu} a_{n\mu}^\dagger \boldsymbol{\sigma}_{\mu\nu} \cdot \mathbf{S}_n a_{n\nu}. \quad (2.7)$$

Next, using the reference Green's function G_0 given by

$$\langle m\mu | G_0(\omega) | n\nu \rangle = \left\langle a_{m\mu} \frac{1}{\omega - K} a_{n\nu}^\dagger \right\rangle_0, \quad (2.8)$$

where $\langle O \rangle_0$ denotes the expectation value of O in the vacuum, we define the t -matrix t^A which represents the multiple scattering of carriers due to an A ion embedded in the effective medium by

$$t_n^A = v_n^A [1 - G_0 v_n^A]^{-1} , \quad (2.9)$$

and t^M due to an M ion by

$$t_n^M = v_n^M [1 - G_0 v_n^M]^{-1} . \quad (2.10)$$

We have omitted suffices of the matrices G , t and v since they are self-evident. The matrix t_n^A (t_n^M) represents the scattering by an isolated potential v_n^A (v_n^M) in the effective medium completely. Note that K , and thus G_0 , includes no localized spin operator. According to the multiple-scattering theory, the total scattering operator T of a random medium, which is related to $G \equiv \left\langle a \frac{1}{\omega - H} a^\dagger \right\rangle_0$ as

$$G = G_0 + G_0 T G_0 , \quad (2.11)$$

is expressed as a series,

$$T = \sum_n t_n + \sum_n t_n G_0 \sum_{m (\neq n)} t_m + \sum_n t_n G_0 \sum_{m (\neq n)} t_m G_0 \sum_{l (\neq m)} t_l + \cdots . \quad (2.12)$$

In the CPA, the condition

$$\langle t_n \rangle_{\text{av}} = 0 \quad \text{for any site } n \quad (2.13)$$

determines the coherent potential $\Sigma_\mu (\mu = \uparrow, \downarrow)$ and we approximate $\langle G \rangle_{\text{av}}$ by G_0 . Here we express the average of a quantity O over the disorder in the system as $\langle O \rangle_{\text{av}}$. Since the present system includes both substitutional disorder and the thermal fluctuations of the localized spin an M site, the average of the t matrix is written as

$$\langle t_n \rangle_{\text{av}} = (1 - x) t_n^A + x \langle t_n^M(\mathbf{S}) \rangle . \quad (2.14)$$

Here $(1 - x)$ and x are the mole fractions of A and M atoms, respectively; $\langle t^M(\mathbf{S}) \rangle$ means the thermal average of t^M over fluctuating localized spin \mathbf{S} . The coherent potential Σ_μ is decided such that the effective scattering of a carrier at the chosen site embedded in the effective medium is zero on average. Since the spin off-diagonal element becomes zero after the average, the condition (the dynamical CPA condition) is given by

$$(1 - x) t_{\uparrow\uparrow}^A + x \langle t_{\uparrow\uparrow}^M(S_z) \rangle = 0 , \quad (2.15a)$$

$$(1 - x) t_{\downarrow\downarrow}^A + x \langle t_{\downarrow\downarrow}^M(S_z) \rangle = 0 . \quad (2.15b)$$

For simplicity, the t matrix elements in the site representation $\langle n\mu | t | n\nu \rangle$ (n is a site index, $\mu, \nu = \uparrow$ or \downarrow) are written as $t_{\mu\nu}$. It is worth noting that in the calculation of $t_{\uparrow\uparrow}^M$ ($t_{\downarrow\downarrow}^M$) the spin flip processes are properly taken into account, and a single t -matrix element $t_{\mu\mu}^M$ depends on both Σ_\uparrow and Σ_\downarrow . Therefore we need to solve Eqs. (2.15a) and (2.15b) simultaneously. Note that the diagonal matrix element $t_{\mu\mu}^M$ involves S_z as an operator, where S_z stands for the z -component of the localized spin. The thermal average over the fluctuating localized spin is taken as

$$\langle t_{\mu\mu}^M(S_z) \rangle = \sum_{S_z=-S}^S t_{\mu\mu}^M(S_z) \exp\left(\frac{hS_z}{k_B T}\right) / \sum_{S_z=-S}^S \exp\left(\frac{hS_z}{k_B T}\right) , \quad (2.16)$$

where h denotes the effective field felt by the localized spins. Since there is one-to-one correspondence between $\langle S_z \rangle$ and the parameter $\lambda \equiv h/k_B T$, we can describe the carrier states in terms of $\langle S_z \rangle$ instead of λ . Note that the thermal average of off-diagonal t -matrix elements $\langle t_{\uparrow\downarrow}^M \rangle_{\text{av}} = \langle t_{\downarrow\uparrow}^M \rangle_{\text{av}} = 0$ because the magnetization is assumed to be along the z -axis. In this work we treat the localized spins classically for simplicity. The actual calculations were performed for $S = 400$.

Throughout this work we assume a model density of states with a semicircular profile whose half-bandwidth is Δ ,

$$\rho(\varepsilon) = \frac{2}{\pi\Delta} \sqrt{1 - \left(\frac{\varepsilon}{\Delta}\right)^2}, \quad (2.17)$$

as the unperturbed density of states. Then the density of states with μ spin $D_\mu(\omega)$ is calculated as

$$\begin{aligned} D_\mu(\omega) &= -\frac{1}{\pi} \text{Im} \langle n_\mu | G(\omega) | n_\mu \rangle_{\text{av}} \cong -\frac{1}{\pi} \text{Im} \langle n_\mu | G_0(\omega) | n_\mu \rangle \\ &= -\frac{1}{\pi} \text{Im} \int_{-\Delta}^{\Delta} d\varepsilon \frac{\rho(\varepsilon)}{\omega - \varepsilon - \Sigma_\mu(\omega)} \end{aligned} \quad (2.18)$$

by using Σ_μ determined by the condition (2.15). In all of the present results we confirmed numerically the sum rule:

$$\int_{-\infty}^{\infty} D_\uparrow(\omega) d\omega = \int_{-\infty}^{\infty} D_\downarrow(\omega) d\omega = 1. \quad (2.19)$$

2.3 The Curie temperature

We calculate the Curie temperature T_c to investigate the condition for the occurrence of ferromagnetism. Throughout this paper we assume that the carriers are degenerate. Then we obtain the density of the carrier with μ spin n_μ and the total energy $E(\langle S_z \rangle)$ as

$$n_\mu = \int_{-\infty}^{\varepsilon_F} D_\mu(\omega) d\omega \quad (2.20)$$

and

$$E(\langle S_z \rangle) = \int_{-\infty}^{\varepsilon_F} \omega [D_\uparrow(\omega) + D_\downarrow(\omega)] d\omega, \quad (2.21)$$

respectively, as functions of the Fermi level ε_F . Here the dependence on $\langle S_z \rangle$ is contained in $D_\mu(\omega)$. Note that $E(\langle S_z \rangle)$ is the sum of the kinetic and the exchange energies. For a fixed value of $\langle S_z \rangle/S$, the total carrier density n ($\equiv n_\uparrow + n_\downarrow$) has one-to-one correspondence with ε_F and therefore $E(\langle S_z \rangle)$ can be expressed as a function of n . The free energy per site of the system is given as

$$F(\langle S_z \rangle) = E(\langle S_z \rangle) - TS, \quad (2.22)$$

where the entropy due to the localized spins is given by

$$\mathcal{S} = xk_B \log \sum_{S_z=-S}^S \exp(\lambda S_z) - xk_B \lambda \langle S_z \rangle. \quad (2.23)$$

The parameter λ is determined so as to minimize $F(\langle S_z \rangle)$ through the condition $\frac{d}{d\lambda} F(\langle S_z \rangle) = 0$. If we expand $F(\langle S_z \rangle)$ in terms of $(\langle S_z \rangle)^2$, T_c is determined as the temperature where the

coefficient of $(\langle S_z \rangle)^2$ vanishes. As is revealed later [see Fig. 20(a)] the energy difference between the ferromagnetic and paramagnetic states,

$E(\langle S_z \rangle) - E(0)$, is approximately proportional to $(\langle S_z \rangle)^2$ up to full polarization at a fixed carrier density. Therefore we fitted the numerical data of $[E(\langle S_z \rangle) - E(0)]/\Delta$ to the expansion

$$\frac{E(\langle S_z \rangle) - E(0)}{\Delta} = -a \left(\frac{\langle S_z \rangle}{S} \right)^2 + b \left(\frac{\langle S_z \rangle}{S} \right)^4 \quad (2.24)$$

and estimated the coefficients a and b . Finally we obtain T_c as

$$\frac{k_B T_c}{\Delta} = \frac{2a}{3x}. \quad (2.25)$$

§3. Carrier states in DMS's

3.1 General consideration

Let us start with confirming that the exchange interaction term, $-I\boldsymbol{\sigma} \cdot \mathbf{S}$, has two energy eigenvalues according to the manner of coupling between the carrier spin and the localized spin. The parallel coupling state (denoted by p) with $2S + 2$ -fold degeneracy has the energy eigenvalue $\varepsilon_p = -IS$, while the antiparallel coupling state (denoted by a) with $2S$ -fold degeneracy has the energy eigenvalue $\varepsilon_a = I(S + 1)$. The classical spin approximation assumes S to be infinite while keeping IS constant. Then the parallel and antiparallel eigenstates have the same degeneracy and their energy eigenvalues have the same absolute value $|IS|$. In this work we adopt the classical spin approximation since the magnitude of the localized spin on a Mn^{2+} ($S = \frac{5}{2}$) is pretty large. It is, therefore, sufficient to appoint the value of the exchange energy IS instead of appointing the values of I and S separately.

In most DMS's, the p - d exchange interaction between a p hole and a localized spin favors antiparallel coupling. The p - d exchange interaction is known to play a crucial role in magnetooptical effects in II-VI-DMS's, and is also believed to cause the carrier-induced ferromagnetism in III-V-DMS's. Hence, keeping the p - d exchange interaction in mind, we assume $IS < 0$ hereafter. The present model is characterized by only two parameters, IS/Δ and E_M/Δ , since we take E_A as the origin ($= 0$) of the energy.

3.2 Result for $IS = -\Delta$ and $E_M = 0$

In the following we show the results for three typical cases of $A_{1-x}M_xB$ -type DMS's, in which 5 % of the nonmagnetic (A) ions are randomly substituted by magnetic (M) ions. The present and next subsections reports typical cases in $E_M = 0$. In Figs. 1 ~ 4 we show the numerical results for $IS = -\Delta$ and $E_M = 0.0$, which is the case where the exchange interaction is so strong that magnetic impurity bands appear. In Fig. 1, the spin-polarized DOSs, $D_\uparrow(\omega)$ and $D_\downarrow(\omega)$, are depicted for various values of $\langle S_z \rangle/S$. In the dilute limit ($x \rightarrow 0$) impurity levels appear at the energies of $\frac{E_a}{\Delta} = \left(\frac{E_M \mp IS}{\Delta} \right) + \frac{1}{4} \left(\frac{\Delta}{E_M \mp IS} \right) = \pm 1.25$. When $x = 0.05$, impurity bands form around the impurity levels. The total number of states of each impurity band is x , irrespectively of $\langle S_z \rangle$. The low (high) energy impurity band corresponds to the antiparallel (parallel) coupling state. The impurity bands are strongly affected by the change in $\langle S_z \rangle$. On the other hand, the host band is negligibly affected. In order to elucidate the origin of the change in the DOS, we calculate the species-resolved DOS. In Fig. 2, we depict the A - and M -site components of the DOS, $(1-x)D_\mu^A(\omega)$ and $x D_\mu^M(\omega)$, where $D_\mu^A(\omega)$ [$D_\mu^M(\omega)$] represents the local DOS with μ spin ($\mu = \uparrow$ or \downarrow) associated with the A (M) ion. The total number of A - and M -site states are $1-x$ and x , respectively. Since

$D_\mu^A(\omega)$ and $D_\mu^M(\omega)$ are normalized

$$D_\mu(\omega) = (1 - x)D_\mu^A(\omega) + xD_\mu^M(\omega) . \quad (3.1)$$

The result shown in Fig. 2 reveals that the impurity state is mainly composed of the M -site states and that the change in the impurity band is mainly ascribed to the change in $D_\mu^M(\omega)$.

Next, we investigate the manner of coupling between the carrier spin and the localized spin. In Fig. 3(a) we show the result for the optical carrier spin polarization $P(\omega)$, where $P(\omega)$ is defined by

$$P(\omega) = \frac{D_\downarrow(\omega) - D_\uparrow(\omega)}{D_\downarrow(\omega) + D_\uparrow(\omega)} . \quad (3.2)$$

The result strongly suggests that

$$P(\omega) \approx +\frac{\langle S_z \rangle_{\text{av}}}{S} \quad \text{in the lower impurity band,} \quad (3.3a)$$

$$P(\omega) \approx -\frac{\langle S_z \rangle_{\text{av}}}{S} \quad \text{in the higher impurity band.} \quad (3.3b)$$

We can deduce the result of Eq. (3.3) by assuming that the carrier spin always couples antiparallel (parallel) to the localized spin in the lower (higher) impurity band. To confirm the above picture, we calculate the spin-coupling strength $Q(\omega)$ defined by (see Appendix)

$$Q(\omega) \equiv -\frac{\langle \delta(\omega - H) \sigma \cdot \mathbf{S} \rangle / S}{\langle \delta(\omega - H) \rangle} \Big|_{M\text{-site}} . \quad (3.4)$$

Thus, $Q(\omega)$ corresponds to $-\langle \cos \theta \rangle$, where θ is the angle between the carrier spin and localized spin at an M site. The result for $Q(\omega)$ shown in Fig. 3(b) clearly indicates that

$$Q(\omega) \approx 1.0 \quad \text{in the lower impurity band,} \quad (3.5a)$$

$$Q(\omega) \approx -1.0 \quad \text{in the higher impurity band.} \quad (3.5b)$$

Above results show that in the lower magnetic impurity band the carrier spin is almost completely antiparallel with the fluctuating localized spin at an M site.

In Fig. 4, we extract the low energy part of the DOS. A magnetic impurity band forms around the impurity level and its DOS has similar shape to the model band. The total number of states in the impurity band per site is equal to x irrespective of the value of $\langle S_z \rangle$. When $\langle S_z \rangle = S$, all states in the impurity band are down-spin states, whereas the impurity band is composed of the same number ($x/2$) of up- and down-spin states when $\langle S_z \rangle = 0$. The impurity band has a larger bandwidth in the ferromagnetic state than in the paramagnetic state. The change in the bandwidth is understood as a result of the change in the effective hopping integral between Mn sites. When the coupling between the localized spin and the carrier spin is strong, the effective hopping between site i and j is reduced in proportion to $\cos \theta_{ij}/2$ where θ_{ij} is the angle between the localized spins at site i and j .²⁵⁾ In a fully polarized ferromagnetic state $\cos \theta_{ij}/2$ is always unity while $\langle \cos \theta_{ij}/2 \rangle = 2/3$ if the localized spins are completely randomly oriented. The result shown in Fig. 3 certifies that Anderson-Hasegawa theory is applicable for the magnetic impurity band in this case. Change in the bandwidth makes the energy of the ferromagnetic state lower than that of the paramagnetic state when n is small. The energy gain increases with increase of n and reaches a maximum at $n \sim x/2$. and then gradually decreases to vanishes at $n \sim x$ as will be shown later.

3.3 The case of $IS = -0.4\Delta$ and $E_M = 0$

Here we discuss the case of the exchange energy $IS = -0.4\Delta$ and the band offset energy $E_M = 0.0$. In this case the acceptor level does not appear in the dilute limit since $|E_M \pm IS| < 0.5\Delta$. To our knowledge no magnetic impurity band has been reported in $A_{1-x}^{\text{II}}\text{Mn}_x\text{B}^{\text{VI}}$ -type DMS's.¹⁾ Therefore the present model with the parameters of $|E_M \pm IS| < 0.5\Delta$ may correspond to II-VI DMS's. Numerical results are presented in Figs. 5 ~ 7. In Fig. 5 the spin-polarized DOS is shown for various values of $\langle S_z \rangle$. As can be seen in Fig. 6(b), the carrier states at the M -site exist in the whole range of band energy. The results for $P(\omega)$ and $Q(\omega)$ shown in Fig. 7 suggest that coupling between the carrier spin and the localized spin is not strong except at the band edges, which is consistent with the weak $\langle S_z \rangle$ dependence of $xD^M(\omega)$ shown in Fig. 6(b). In Fig. 5 the Fermi level ε_F for $n = 0.05$ is indicated by an arrow.

3.4 Property of ferromagnetism in $E_M = 0$

In order to study the nature of carrier-induced ferromagnetism, we first calculate the Curie temperature T_c in a very simple way. We estimate T_c using the energy of the paramagnetic state $E(0)$ and that of the completely ferromagnetic state $E(S)$ as

$$k_B T_c = \frac{2}{3x} [E(0) - E(S)] \quad (3.6)$$

assuming $b = 0$ in Eq. (2.24). Note that the CPA condition (2.15) results in a cubic equation when $\langle S_z \rangle_{\text{av}} = S$ and a quartic equation when $\langle S_z \rangle_{\text{av}} = 0$.²⁶⁻²⁸⁾

In Fig. 8 the result for T_c is presented as a function of n for various values of IS/Δ . We immediately notice that there are two different types of behavior in T_c as a function of n depending on the size of $|IS|/\Delta$. When $|IS|/\Delta$ is small ($|IS|/\Delta \lesssim 0.3$), the ferromagnetism occurs over a wide range of n . The Curie temperature gradually increases with the increase in n and reaches a broad maximum. Then it gently decreases and vanishes at a critical value n_c . The maximum T_c stays at a low value, and n_c is much larger than $x (= 0.05)$. On the other hand, when $|IS|/\Delta$ is large ($|IS|/\Delta \gtrsim 0.7$), the ferromagnetism occurs in a narrow range of n ($\lesssim x$). The T_c rises steeply and reaches a maximum at $n_x \approx x/2$, and then it decreases rapidly. The maximum T_c is high and n_c is less than but nearly equal to x . These two different features can be seen clearly in Fig. 9 as well, where n_c and the maximum T_c are depicted as functions of n . The carrier density n_x at which T_c reaches the maximum is also shown. Two different characteristic features were also recognized in the phase diagrams obtained in an earlier study with Ising localized spins.²²⁾ When $|IS|/\Delta \lesssim 0.3$, the maximum T_c is approximately proportional to $(IS/\Delta)^2$. This suggests that in the range of $|IS|/\Delta \lesssim 0.3$ the perturbative treatment on IS/Δ is available and the RKKY-like mechanism is expected to operate for a moderate carrier density. With further increase in $|IS|/\Delta$ the maximum T_c rises rapidly ($0.3 \lesssim |IS|/\Delta \lesssim 0.7$), and then tends to saturate. For $|IS|/\Delta \gtrsim 0.7$, ferromagnetism is induced only when $n \lesssim x$ and the maximum T_c realizes at $n_x \cong x/2$. The case with $IS = -\Delta$ studied in §3.2 belongs to this region and therefore the mechanism for ferromagnetism is understood from the argument above. As was shown in Fig. 4 the width of the magnetic impurity band increases with increase of magnetization according to Anderson-Hasegawa mechanism. It leads to the energy gain in ferromagnetic state if the Fermi level lies in the impurity band. This is essentially the same mechanism with that of the double-exchange interaction which causes ferromagnetism in mixed valency transition metal oxides such as $(\text{LaCa})\text{MnO}_3$.^{24, 25)} Therefore we may say that the 'double-exchange (DE)-like' mechanism for ferromagnetism is operative in the impurity band when $|IS|/\Delta \gtrsim 0.7$. Here we point out that

the magnetic impurity levels appear when $|IS|/\Delta > 0.5$ if $E_M = 0$. Therefore we conclude that the DE-like mechanism in a magnetic impurity band becomes dominant when $|IS|/\Delta \gtrsim 0.7$. In II-VI DMS's, the magnetic impurity level does not appear as illustrated in Fig. 5, in which the parameters, $|IS|/\Delta = 0.4$ and $E_M = 0$, were employed. Therefore, we may conclude that the DE-like mechanism is not relevant to the ferromagnetism in II-VI DMS's.

To confirm above picture, we try to estimate T_c in the strong exchange interaction limit through a simple argument. In this limit the impurity band has the same shape of the model density of states $\rho(\omega)$ defined by Eq. (2.17) around the impurity level E_a . In the completely ferromagnetic case the DOS of the impurity band has a finite value at the energies of $E_a - \sqrt{x}\Delta \leq \omega \leq E_a + \sqrt{x}\Delta$ and is given by

$$D_F(\omega) = \sqrt{x} \times \rho\left(\frac{\omega - E_a}{\sqrt{x}}\right). \quad (3.7)$$

In the paramagnetic case the DOS of the impurity band has a finite value at the energies of $E_a - \sqrt{x/2}\Delta \leq \omega \leq E_a + \sqrt{x/2}\Delta$ and is given by

$$D_P(\omega) = 2 \times \sqrt{x/2} \times \rho\left(\frac{\omega - E_a}{\sqrt{x/2}}\right), \quad (3.8)$$

where the factor 2 is due to up- and down-directions of the carrier spin. The result for T_c based on the assumption is inserted in Fig. 8 as a 'LIMIT'. The maximum T_c is estimated to be

$$k_B T_c = \frac{2(2 - \sqrt{2})}{9\pi} \sqrt{x}\Delta, \quad (3.9)$$

at $n = x/2$. The value of the maximum T_c ($= 0.0093\Delta$) for $x = 0.05$ is pointed by an arrow in Fig. 9.

It is worth noting that the Zener double-exchange mechanism for ferromagnetism is usually understood to be effective only when the exchange energy is larger than the width of the carrier band (or $|IS| \gtrsim 2\Delta$) in the case where magnetic ions sit on each site. In the present case the exchange energy is not larger than the width of the model band. Nevertheless the 'DE-like' mechanism functions because the magnetic impurity bandwidth is smaller than the exchange energy (or $|IS| \gtrsim \sqrt{2x}\Delta$).

3.5 Effect of the attractive potential

We study here the role of the attractive potential in order to elucidate the origin of the carrier-induced ferromagnetism in III-V-based DMS's. Figures 10 ~ 12 show the results for the case where $IS = -0.4\Delta$ and $E_M = -0.6\Delta$. Although the strength of the exchange coupling is same as that in §3.3, an impurity band appears due to an attractive nonmagnetic local potential $E_M = -0.6\Delta$. Furthermore, we find a strong similarity between the low energy part of DOS in Fig. 1 ($IS = -\Delta$ and $E_M = 0$) and that in Fig. 10 ($IS = -0.4\Delta$ and $E_M = -0.6\Delta$). The similarity is due to the fact that the impurity level has the same energy, $E_a = -1.25\Delta$, which is determined by the effective attractive potential $E_M + IS$. When $\langle S_z \rangle = 0$ a magnetic impurity band with $x/2$ down- and up-spin states forms around the impurity level in both cases. Thus the impurity bands in both cases have a strong similarity although they do not completely agree with each other. When $\langle S_z \rangle = S$, the down-spin bands agree completely with each other in both cases because the DOS's were determined only by the energy of antiparallel coupling $E_M + IS$. The up-spin impurity bands

are completely suppressed in both cases and the states merge into the host band. Thus, for up-spin as well, we find a similarity in the low energy part of the DOS's shown in Figs. 1 and 10. From the similarity in the low energy part of the DOS, we may expect that ferromagnetism occurs through the same mechanism in both cases. In Fig. 13 the effect of the nonmagnetic potential E_M on T_c is presented for IS fixed to be -0.4Δ . The impurity level appears for $E_M < -0.1\Delta$ in this case. When $E_M \gtrsim 0.0$ the T_c stays low and n_c is much larger than x , while for $E_M \lesssim -0.2\Delta$ high T_c is realized and n_c is less than x . In the latter region the DE-like mechanism becomes in effect. Figure 14 shows how the maximum T_c as well as n_c varies with E_M and IS . The result reveals that the attractive nonmagnetic potential E_M extends the region where the DE-like mechanism is effective and enhances maximum T_c . The criterion for the DE-like mechanism to operate is roughly estimated to be $IS + 0.4E_M \lesssim -0.6\Delta$.

§4. Summary and Discussions

In the present study we applied the dynamical CPA to a simple model in order to investigate the carrier states of DMS's in a systematic way. The present results reveal that a magnetic impurity band forms separate from the host band when the effective attractive potential is strong enough. In such a case the spin of a carrier in the impurity band couples very strongly with the localized spin at a magnetic impurity site. Then the hopping of the carriers among the magnetic sites aligns the localized spins parallel through the DE-like mechanism. The effective attractive potential is determined by the sum of the non-magnetic attractive potential and the exchange interaction. Therefore, the non-magnetic potential substantially enhances the effect of the exchange interaction. This mechanism works even in the case where the impurity band is not completely separate from the host band. This is the case in III-V-based DMS's, where the exchange interaction alone is not strong enough to make a pronounced impurity band. On the other hand, the absence of non-magnetic attractive potential in II-VI-based DMS's suppresses the magnetic impurity band and therefore the appearance of strong ferromagnetism.

Here we compare the Zener double-exchange (DE) mechanism and the present DE-like mechanism that occurs in the magnetic impurity band. Zener originally proposed the DE interaction for (La,Ca)MnO₃ where 3d-holes hop among the magnetic ions sitting on the regular lattice sites.³⁴⁾ Therefore it might be usually understood that DE mechanism is only relevant to hopping of the 3d holes in (Ga,Mn)As. The DE mechanism for ferromagnetism is, in fact, works quite generally in cases where the kinetic energy (or the bandwidth) of a carrier is not greater than the exchange energy between a carrier spin and a localized spin. It originates from the effective reduction of the hopping amplitude between sites with localized spins which are not parallel with each other. The reduction is in proportion to $\cos \theta/2$ where θ is the relative angle between the localized spins.²⁵⁾ Only condition required for this reduction is a very strong exchange coupling between carrier spins and localized spins. If it is satisfied, carriers may have any character and the localized spins can be arranged randomly. Even localized spins are not necessary for this mechanism if strong Hund couplings are working between carrier spins on the same site.^{35,36)}

In the case of III-V based DMS's, carriers are considered to have 4p character^{6,9)} and therefore the bandwidth (~ 4 eV) is not larger than the exchange energy ($IS = 0.6 \sim 0.8$ eV). However the attractive interaction between the carrier and a Mn²⁺ ion helps for the ion to bind the carrier, and in consequence the carrier moves in a narrow impurity band. The effective bandwidth for a carrier is that of the impurity band and it is smaller than the exchange energy. The DE mechanism becomes in effect even if the impurity band is not completely separated from the host band. We call this mechanism "DE-like" mechanism in order to avoid confusion with the argument assuming d

holes.¹⁷⁾ We note here that no Mn^{3+} (d^4 configuration) states have been experimentally detected in $(\text{Ga},\text{Mn})\text{As}$.^{3,5,6,13,37)} All these experimental observations rather suggests the picture that the fixed valence state Mn^{2+} ($S = 5/2$) is realized in $(\text{Ga},\text{Mn})\text{As}$. The absence of the attractive potential suppresses the appearance of a magnetic impurity band and therefore the DE-like mechanism does not work in II-VI-based DMS's.

The results for the n dependence of the energy gain and T_c , shown in Fig. ?? are well explained on the basis of the DE-like mechanism. Recently Hayashi *et al.* reported that heat treatments (annealing) could vary the hole concentration n_h while holding x constant.¹⁵⁾ They reported in a sample with a nominal Mn content of 5 % that T_c increased from $\sim 80\text{K}$ to $\sim 95\text{K}$ and then decreased again to $\sim 80\text{K}$ when n_h was increased from 6.1 to 6.8 and then $7.2 \times 10^{19} \text{ cm}^{-3}$. The carrier concentration in these cases are 2.7, 3.1 and 3.3%, respectively. The result implies that T_c takes its maximum at $n_h \sim 0.6x$ in the sample, while the present theory predicts a maximum at $\sim 0.3x$ as is shown in Fig. 20(b). Study of a more realistic model taking into other effects and/or more detailed experimental investigations are necessary to clarify this discrepancy.

Although we assumed the p -holes with a wide bandwidth for carriers, the present result is in contrast with the RKKY argument which assumes the free-carrier picture.¹⁶⁾ Infrared optical absorption measurements have recently revealed that the hole wave functions are nearly localized and the transport should be more or less hopping-like even in the most metallic $\text{Ga}_{1-x}\text{Mn}_x\text{As}$.^{38,39)} The nearly bound-hole picture is consistent with the present result that the p hole in the band tail prefers to stay on Mn sites [see Fig. ??(c)].

Although the exchange interaction between p hole and d spin is experimentally established to be *antiferromagnetic*,^{6,12,13)} the exchange interaction was reported to be *ferromagnetic* in an early study on the polarized magnetoreflexion.⁴⁰⁾ In our result shown in Fig. 4, the bottom of the down-spin magnetic impurity band shifts to the lower energy side with increase in $\langle S_z \rangle$, whereas that of the host band shifts to the higher energy side. It is also worth noting that $Q(\omega) \approx -1.0$ at the bottom of the host band (see Fig. 3 (b)). These indicate that the ferromagnetic spin coupling occurs at the bottom of the host band, contrary to the antiferromagnetic spin coupling in the magnetic impurity band. If we interpret that the optically observed band edge is not that of the impurity band but that of the host band, the present result may explain the experimental observation. A simple calculation based on the present approach consistently explains the apparent ferromagnetic exchange interaction experimentally observed. Details will be published elsewhere.⁴¹⁾

Next, we briefly mention the quantum effect of the localized spin that is ignored in the present work. When the calculations are done for the quantum spins with finite S , the total number of states in a impurity band is not x but $2x(S+1)/(2S+1)$ for parallel coupling and $2xS/(2S+1)$ for antiparallel coupling, respectively. The result is valid as long as the band is almost empty. The many body effect, however, may change the situation.⁴²⁾ Therefore, although the present result suggests that T_c might be multiplied by a factor $\sqrt{2(S+1)/(2S+1)}$ or $\sqrt{2S/(2S+1)}$ in the strong coupling limit, the effect of quantum spin is still unclear at the present stage.

The Curie temperature obtained by using the model with randomly distributed Ising spins²²⁾ is about three times larger than the present result. The reason may be due to the fact that the spin-flip effect is not taken into account in their theory.

Throughout this work, the carriers were assumed to be degenerate. Recently the dynamical mean-field theory^{43,44)} was applied to the present model. The result for T_c is almost the same as the present result, which suggests that the assumption of the degenerate carriers is reasonable. The result will be published elsewhere together with the result of the temperature dependence of magnetization.⁴⁵⁾

The present model has succeeded in explaining the fundamental mechanism of the carrier-induced ferromagnetism in III-V based DMS's. There are, however, many features which exist in the real DMS's but are not taken into account. Those are multi-band effects, the band anisotropy, the spin-orbit coupling, p - d hybridization, the long-range character of the Coulomb potential, the direct antiferromagnetic exchange interaction between Mn ions and so on. These issues remain for future study.

-
- 1) J. K. Furdya: J. Appl. Phys. **64**(1988) R29.
 - 2) H. Ohno: J. Magn. Magn. Mater. **200** (1999) 200.
 - 3) M. Linnarsson, E. Janzen, B. Monemar, M. Kleverman, and A. Thilderkvist: Phys. Rev. B **55** (1997) 6938.
 - 4) Y. Iye, A. Oiwa, A. Endo, S. Katsumoto, F. Matsukura, A. Shen, H. Ohno, and H. MuneKata: Mater. Sci. Eng. B **63** (1999) 88.
 - 5) H. Ohldag, V. Solinus, F. U. Hillebrecht, J. B. Goedkoop, M. Finazzi, F. Matsukura, and H. Ohno: Appl. Phys. Lett. **78** (2001) 1691.
 - 6) J. Okabayashi, A. Kimura, O. Rader, T. Mizokawa, A. Fujimori, T. Hayashi, and M. Tanaka: Phys. Rev. B **58** (1998) R4211.
 - 7) J. Okabayashi, A. Kimura, T. Mizokawa, A. Fujimori, T. Hayashi, and M. Tanaka: Phys. Rev. B **59** (1999) R2486.
 - 8) J. Okabayashi, A. Kimura, O. Rader, T. Mizokawa, A. Fujimori, T. Hayashi, and M. Tanaka: Phys. Rev. B **64** (2001) 125304.
 - 9) Y. Ishiwata, M. Watanabe, R. Eguchi, T. Takeuchi, Y. Harada, A. Chainani, S. Shin, T. Hayashi, Y. Hashimoto, S. Katsumoto, and Y. Iye: Phys. Rev. B **65** (2002) 233201.
 - 10) M. Shirai, T. Ogawa, I. Kitagawa, and N. Suzuki: J. Magn. Magn. Mater. **177-181** (1998) 1383.
 - 11) J. H. Park, S. K. Kwon, and B. I. Min: Physica B **281 & 282** (2001) 703.
 - 12) K. Ando, T. Hayashi, M. Tanaka, and A. Twardowski: J. Appl. Phys. **53** (1998) 6548.
 - 13) J. Szczytko, M. Mac, A. Twardowski, F. Matsukura, and H. Ohno: Phys. Rev. B **59** (1999) 12935.
 - 14) J. Okabayashi, T. Mizokawa, D. D. Sarma, A. Fujimori, T. Slupinski, A. Oiwa, and H. MuneKata: Phys. Rev. B **65** (2002) 161203(R).
 - 15) T. Hayashi, Y. Hashimoto, S. Katsumoto, and Y. Iye: Appl. Phys. Lett. **78** (2001) 1691.
 - 16) F. Matsukura, H. Ohno, A. Shen, and Y. Sugawara: Phys. Rev. B **57** (1998) R2037.
 - 17) H. Akai: Phys. Rev. Lett. **81** (1998) 3002.
 - 18) J. Köig, H-H. Lin, and A. H. MacDonald: Phys. Rev. Lett. **84** (2000) 5628.
 - 19) J. Inoue, S. Nonoyama, and H. Itoh: Phys. Rev. Lett. **85** (2000) 4610.
 - 20) T. Dietl, H. Ohno, F. Matsukura, J. Cibert, and D. Ferrand: Science **287** (2000) 1019.
 - 21) G. Bouzerar and T. P. Pareek: Phys. Rev. B **65** (2002) 153203.
 - 22) M. Yagi, and Y. Kayanuma: J. Phys. Soc. Jpn. **71** (2002) 2010.
 - 23) M. Takahashi and K. Kubo: Phys. Rev. B **66** (2002) 153202.
 - 24) C. Zener: Phys. Rev. **81** (1951) 403.
 - 25) P. W. Anderson and H. Hasegawa: Phys. Rev. **100** (1955) 675.
 - 26) M. Takahashi: Phys. Rev. B **60** (1999) 15858.
 - 27) M. Takahashi: J. Phys.: Condens. Matter. **13** (2001) 3433.
 - 28) M. Takahashi: J. Phys. Soc. Jpn. **70** (2001) 2224.
 - 29) K. Kubo: J. Phys. Soc. Jpn. **36** (1974) 32.
 - 30) M. Takahashi and K. Mitsui: Phys. Rev. B **54** (1996) 11298.
 - 31) J. Okabayashi, A. Kimura, O. Rader, T. Mizokawa, A. Fujimori, T. Hayashi, and M. Tanaka: Physica E **10** (2001) 192.
 - 32) A. Oiwa, S. Katsumoto, A. Endo, M. Hirakawa, M. Iye, H. Ohno, F. Matsukura, A. Shen, and Y. Sugawara: Solid State Comm. **103** (1997) 209.

- 33) A. Oiwa, S. Katsumoto, A. Endo, M. Hirakawa, M. Iye, F. Matsukura, A. Shen, Y. Sugawara, and H. Ohno: *Physica B* **249-251** (1998) 775.
- 34) G. H. Jonker and J. H. Van Santen: *Physica* **16** (1950) 337; J. H. Van Santen and G. H. Jonker: *ibid* **16** (1950) 599.
- 35) T. Momoi and k. Kubo: *Phys. Rev. B* **58** (1998) R567.
- 36) H. Sakamoto, T. Momoi and K. Kubo: *Phys. Rev. B* **65** (2002) 22403.
- 37) J. Szczytko, A. Twardowski, K. Świątek, M. Palczewska, M. Tanaka, T. Hayashi, and K. Ando: *Phys. Rev. B* **60** (1999) 8304.
- 38) K. Hirakawa, S. Katsumoto, T. Hayashi, Y. Hashimoto, and Y. Iye: *Phys. Rev. B* **65** (2002) 193312.
- 39) S. Katsumoto, T. Hayashi, Y. Iye, Y. Ishiwata, M. Watanabe, R. Eguchi, T. Takeuchi, Y. Harada, S. Shin, and K. Hirakawa: *Mater. Sci. Eng. B* **84** (2001) 88.
- 40) J. Szczytko, M. Mac, A. Stachow, A. Twardowski, P. Becla, and J. Tworzydło: *Solid State Comm.* **99** (1996) 927.
- 41) M. Takahashi: in preparation.
- 42) D. M. Edwards, A. C. M. Green, K. Kubo: *J. Phys: Condens. Matter* **11** (1999) 2791.
- 43) A. Georges, G. Kotliar, W. Krauth and M. J. Rozenberg: *Rev. Mod. Phys.* **68** (1996) 13.
- 44) N. Furukawa: in *Physics of Manganites*, eds. Kaplan-Mahanti (Plenum, NY), (1999) 1.
- 45) N. Furukawa and M. Takahashi: in preparation.

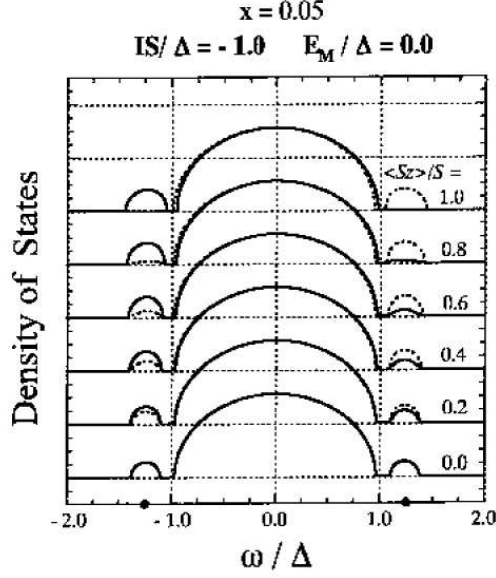


Fig. 1. The result for the DMS with $IS = -\Delta$ and $E_M = 0$. The density of states (DOS) as a function of ω/Δ for various values of $\langle S_z \rangle/S$. Solid line is for down-spin carrier, and dotted line is for up-spin carrier. The impurity levels $E_a = \pm 1.25\Delta$ are indicated by dots on the abscissa.

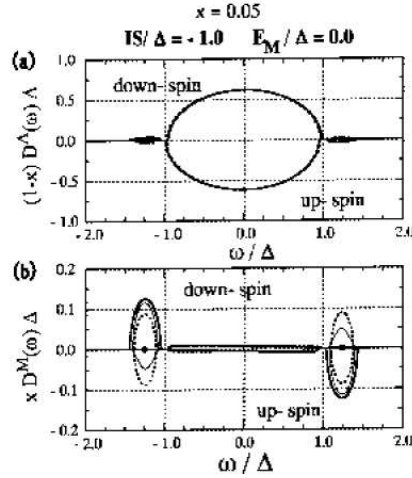


Fig. 2. The results for the DMS with $IS = -\Delta$ and $E_M = 0$. (a) A -site component of the DOS, $(1-x)D_{\downarrow}^A(\omega)\Delta$ and $-(1-x)D_{\uparrow}^A(\omega)\Delta$. (b) M -site component of the DOS, $x D_{\downarrow}^M(\omega)\Delta$ and $-x D_{\uparrow}^M(\omega)\Delta$. The thick, thin and dotted lines represent the cases of $\langle S_z \rangle/S = 1.0, 0.5$ and 0.0 , respectively. Note the difference in the scale of vertical axes between (a) and (b).

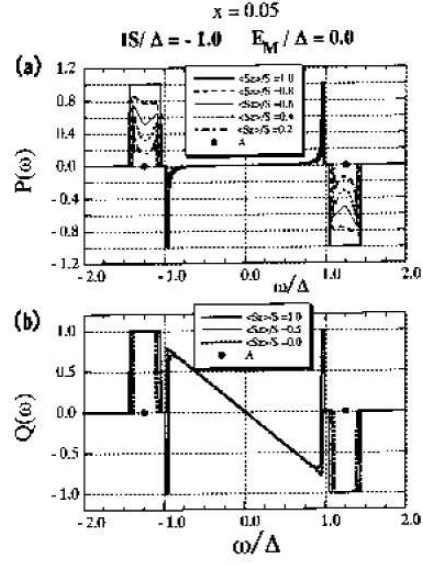


Fig. 3. The result for the DMS with $IS = -\Delta$ and $E_M = 0$. (a) Optical carrier-spin polarization $P(\omega)$ for $\langle S_z \rangle/S = 1.0, 0.8, 0.6, 0.4, 0.2$ and 0.0 . (b) Spin-coupling strength $Q(\omega)$. The thick, thin and dotted lines represent the cases of $\langle S_z \rangle/S = 1.0, 0.5$ and 0.0 , respectively. The impurity levels $E_a = \pm 1.25\Delta$ are indicated by dots on the abscissa.

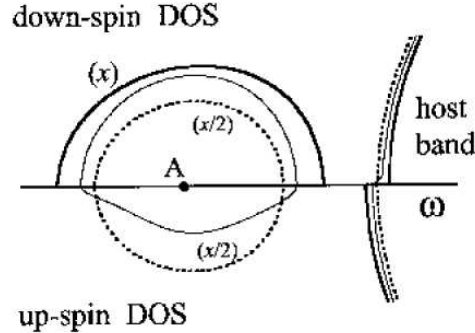


Fig. 4. The DOS of the impurity band in the case of $IS/\Delta = -1.0$ and $E_M = 0$. The thick, thin and dotted lines represent the cases of $\langle S_z \rangle/S = 1.0, 0.5$ and 0.0 , respectively. The dot A indicates the impurity level for $x \rightarrow 0$.

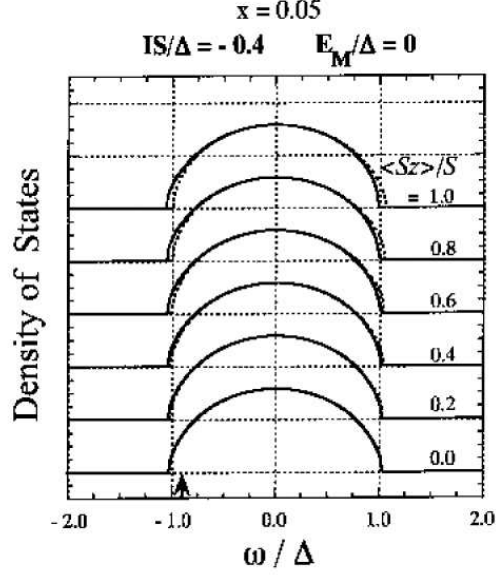


Fig. 5. The result for $IS = -0.4\Delta$ and $E_M = 0$. The DOS as a function of ω/Δ for various values of $\langle S_z \rangle/S$. Solid line is for down-spin carrier, and dotted line is for up-spin carrier. The arrow points to the Fermi level ε_F/Δ for $n = x$ ($= 0.05$).

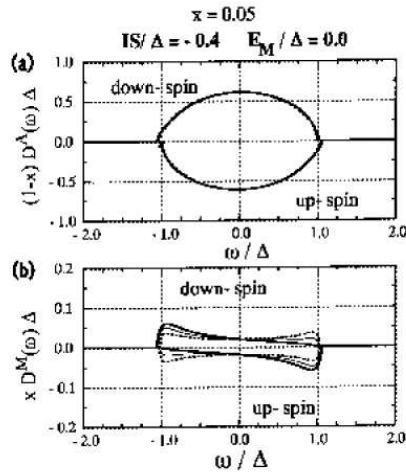


Fig. 6. The result for the DMS with $IS = -0.4\Delta$ and $E_M = 0$. (a) A -site component of the DOS, $(1-x)D_{\downarrow}^A(\omega)\Delta$ and $-(1-x)D_{\uparrow}^A(\omega)\Delta$. (b) M -site component of the DOS, $xD_{\downarrow}^M(\omega)\Delta$ and $-xD_{\uparrow}^M(\omega)\Delta$. The thick, thin and dotted lines represent the cases of $\langle S_z \rangle/S = 1.0, 0.5$ and 0.0 , respectively.

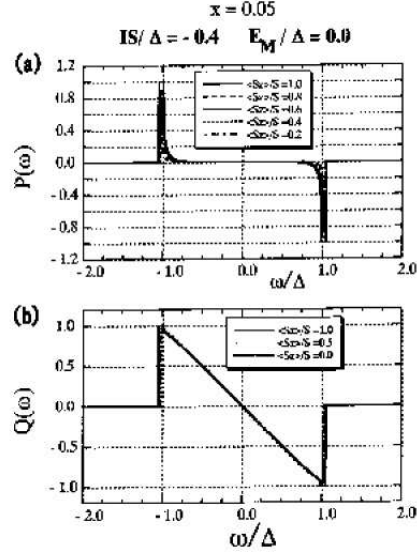


Fig. 7. The result for the DMS with $IS = -0.4\Delta$ and $E_M = 0$. (a) optical carrier-spin polarization $P(\omega)$, (b) spin-coupling strength $Q(\omega)$.

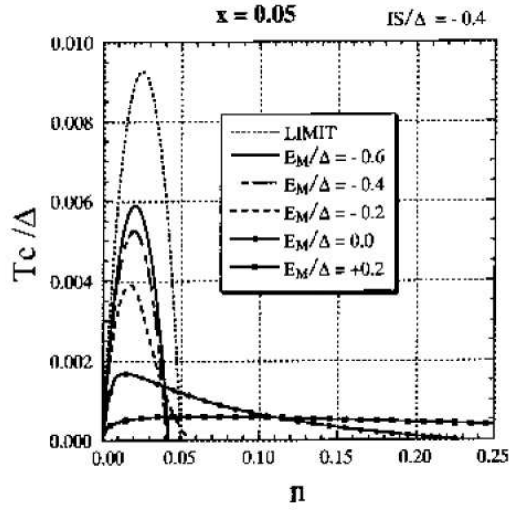


Fig. 8. The result for Curie temperature T_c/Δ as a function of carrier density n for various values of IS/Δ with $x = 0.05$ and $E_M = 0$. The result based on the assumption that an impurity band is similar shape of the model band is drawn as 'LIMIT' (see text).

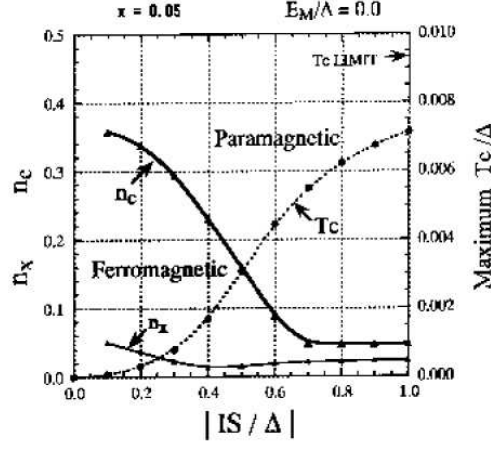


Fig. 9. Phase diagram for $E_M = 0$ and $x = 0.05$. The critical value n_c (solid line; left scale) and the maximum T_c (dotted line; right scale) are presented as a function of $|IS|/\Delta$. The carrier density n_x at which T_c reaches the maximum is included (solid line; left scale).

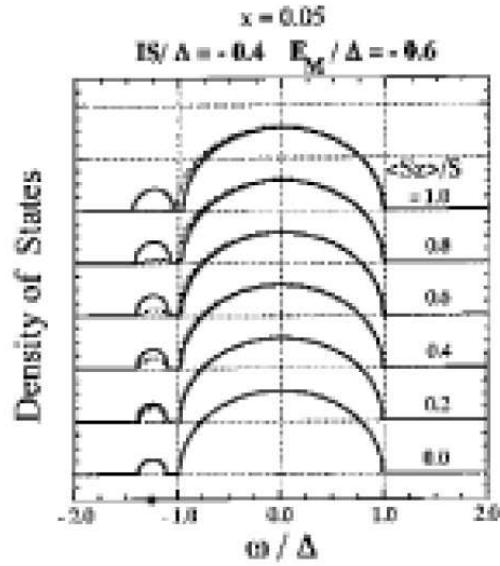


Fig. 10. The result for the DMS with $IS = -0.4\Delta$ and $E_M = -0.6\Delta$. The DOS is plotted as a function of ω/Δ for various values of $\langle S_z \rangle/S$. Solid line is for down-spin carrier, and dotted line is for up-spin carrier. The impurity level $E_a = -1.25\Delta$ is indicated by the dot on the abscissa.

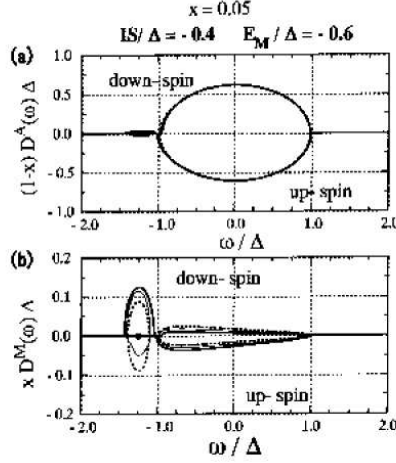


Fig. 11. The result for the DMS with $IS = -0.4\Delta$ and $E_M = -0.6\Delta$: (a) A -site component of the DOS, $(1-x)D_{\downarrow}^A(\omega)\Delta$ and $-(1-x)D_{\uparrow}^A(\omega)\Delta$, (b) M -site component of the DOS, $xD_{\downarrow}^M(\omega)\Delta$ and $-xD_{\uparrow}^M(\omega)\Delta$. The thick, thin and dotted lines represent the cases of $\langle S_z \rangle/S = 1.0, 0.5$ and 0.0 , respectively.

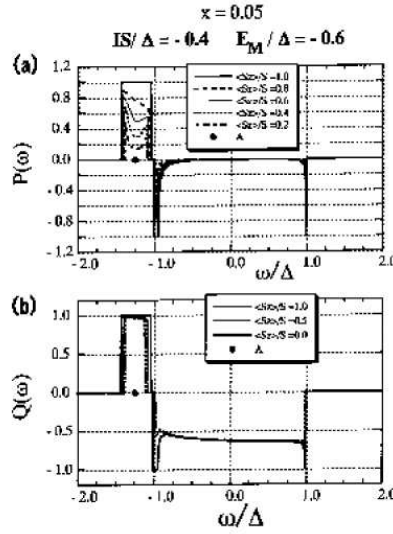


Fig. 12. The result for the DMS with $IS = -0.4\Delta$ and $E_M = -0.6\Delta$: (a) optical carrier-spin polarization $P(\omega)$, (b) spin-coupling strength $Q(\omega)$. The impurity level $E_a = -1.25\Delta$ is indicated by a dot on the abscissa.

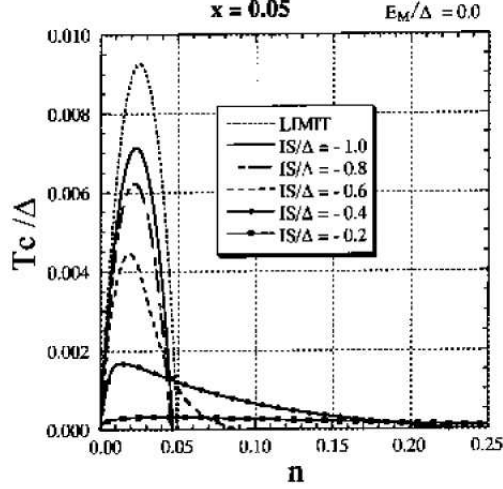


Fig. 13. The result for T_c/Δ as a function of n for various values of E_M/Δ with $x = 0.05$ and $IS = -0.4\Delta$. The result of 'LIMIT' is included (see text).

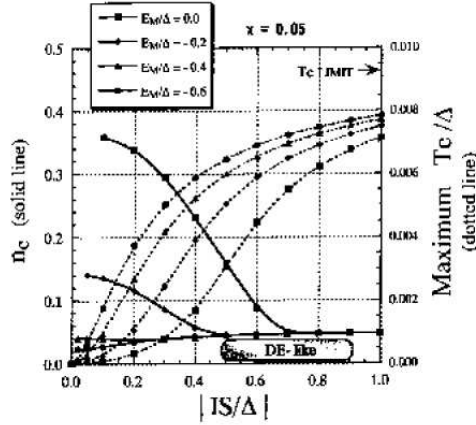


Fig. 14. Phase diagram for various values of E_M/Δ . The critical value n_c (solid line; left scale) and the maximum T_c (dotted line; right scale) are presented as a function of $|IS|/\Delta$ for various values of E_M/Δ .